Numerical tests of the weak pressure gradient approximation

David M. Romps

Dept. of Earth and Planetary Science, University of California, Berkeley

Earth Sciences Division, Lawrence Berkeley National Laboratory Berkeley, California, USA

Corresponding author address:

David M. Romps, Department of Earth and Planetary Science,

377 McCone Hall,

University of California, Berkeley, CA 94720

E-mail:romps@berkeley.edu

ABSTRACT

Cloud-resolving simulations of convection over a surface-temperature hot spot are used to evaluate the weak-pressure-gradient (WPG) and weak-temperature-gradient (WTG) approximations. The premise of the relaxed form of WTG – that vertical velocity is equal to buoyancy times a positive timescale – is found to be violated by thick layers of negative buoyancy in steady-state ascent. The premise of WPG – that horizontal divergence and pressure anomalies are colocated – is validated by these simulations. When implemented in a cloud-resolving model, WPG replicates buoyancy transients exceptionally well, including the adiabatic lifting of air below buoyancy anomalies. WTG captures neither this effect nor the associated triggering of moist convection. For steady states, WTG produces vertical velocity profiles that are too top-heavy. On the other hand, WPG generates velocity profiles that closely match fully-resolved hot-spot simulations. Taken together, the evidence suggests that WPG is a relatively accurate method for parameterizing supra-domain-scale (SDS) dynamics.

1. Introduction

Despite continuing increases in computational power, it will be a long time before the full range of the atmosphere's dynamical scales can be resolved in a single simulation. For example, to perform a climatological simulation of the atmosphere that explicitly resolves scales from 1 mm to 40,000 km would require a computer roughly 10^{20} times more powerful than today's supercomputers. This means that parameterizations will be required in some form at least until the latter half of this century, or longer if Moore's Law falters.

Broadly speaking, dynamical parameterizations fall into two categories: parameterizations of sub-grid-scale (SGS) dynamics and parameterizations of supra-domain-scale (SDS) dynamics. This study addresses the latter. In particular, the focus here is on computational domains that include all of the largest relevant scales in the vertical (e.g., from the surface up into the stratosphere), but do not include all of the largest relevant scales in the horizontal (e.g., a limited-area horizontal domain). This configuration is of interest because it is typical of cloud-resolving simulations.

There are two main methods for parameterizing large-scale SDS dynamics governing the interaction between an atmospheric column and its environment. One is the weak-temperature-gradient (WTG) approximation, in which the temperature of the column is relaxed to that of the environment (e.g., Sobel and Bretherton 2000; Raymond and Zeng 2005; Raymond 2007; Sessions et al. 2010; Wang and Sobel 2011, 2012). The other is the weak-pressure-gradient (WPG) approximation, in which the pressure of the column is relaxed to that of the environment (e.g., Nilsson and Emanuel 1999; Raymond and Zeng 2000; Shaevitz and Sobel 2004; Kuang 2008; Caldwell and Bretherton 2009; Blossey et al. 2009; Kuang 2011). Romps (2012) studied analytical solutions to WTG and WPG in the context of linearized Boussinesq equations and found several reasons why WPG might be more accurate than WTG when implemented in a cloud-resolving model.

Here, WTG and WPG are subjected to both *a priori* and *a posteriori* tests with a cloud-resolving model. In the *a priori* test, a cloud-resolving simulation is performed on a domain that is sufficiently large to resolve all the largest relevant scales. The underlying premises of WTG and WPG are then evaluated in this large-domain simulation. In the *a posteriori* tests, the WTG and WPG schemes are implemented as SDS parameterizations in small-

domain simulations, which are then compared against large-domain simulations. Section 2 describes the implementation of WTG and WPG in a cloud-resolving model. The *a priori* tests of these schemes are performed in section 3 by simulating a sea-surface-temperature (SST) hot spot on a large bowling-alley domain. Section 4 describes an *a posteriori* test of WTG and WPG in the case of steady-state ascent over an SST hot spot. Section 5 describes an *a posteriori* test of WTG and WPG in the case of a transient buoyancy perturbation. A summary of the conclusions is given in section 6.

2. Implementation of WTG and WPG

For the implementation of WTG, a vertical velocity $w(z,t)$ is calculated following Raymond and Zeng (2005) as

$$w(z,t) \;=\; \begin{cases} \dfrac{\bar{\theta}_v(z,t) - \theta_{v0}(z)}{\tau \max\left[\gamma, \partial_z \theta_{v0}(z)\right]} & z \geq h \\ \\ \dfrac{z}{h} w(h,t) & z < h \end{cases} , \tag{1}$$

where $h = 1$ km, $\gamma = 0.01$ K/km, θ_v is virtual potential temperature, a bar denotes a horizontal average over the column, a subscript 0 denotes a reference profile, and the timescale τ is a parameter of the scheme. This is then converted to a horizontal divergence $\delta(z,t)$ according to

$$\delta(z,t) \;=\; -\frac{1}{\bar{\rho}(z,t)} \partial_z \left[\bar{\rho}(z,t) w(z,t)\right] . \tag{2}$$

For $\tau > 0$, this is the relaxed form of WTG; strict WTG, as formulated by Sobel and Bretherton (2000), is recovered by setting $\tau = 0$. For the implementation of WPG, the

horizontal divergence is calculated using the prognostic WPG method of Romps (2012),

$$\partial_t \delta(z,t) \;=\; \frac{1}{L^2}\frac{\bar{p}(z,t)-p_0(z)}{\bar{\rho}(z,t)} - \alpha^* \delta(z,t)\,, \tag{3}$$

where the timescale $1/\alpha^*$ and the length scale L are parameters of the scheme.

When WTG and WPG are implemented in a fully compressible model, the divergence δ is used to calculate tendencies of density, water vapor, and temperature as

$$\partial_t \rho(\vec{x},t) \;=\; -\rho(\vec{x},t)\delta(z,t) + \ldots \tag{4}$$

$$\partial_t \big[\rho(\vec{x},t) q_v(\vec{x},t)\big] \;=\; -\rho(\vec{x},t)\delta(z,t)\Big\{q_v(\vec{x},t) + c(z,t)\big[q_{v0}(z) - q_v(\vec{x},t)\big]\Big\} + \ldots \tag{5}$$

$$\partial_t \big[\rho(\vec{x},t) T(\vec{x},t)\big] \;=\; -\rho(\vec{x},t)\delta(z,t)\Big\{T(\vec{x},t) + c(z,t)\big[T_0(z) - T(\vec{x},t)\big]\Big\} + \ldots\,. \tag{6}$$

Note that there is no need to add an explicit term corresponding to vertical advection by w since equation (4) generates a mean vertical velocity equal to w in the fully compressible model. With $c = 0$, these expressions neglect the effect of advection generated by convergence over a finite-sized domain. For lack of a better term, we will refer to this advective tendency as "convergent advection". For $c = 1/2 - \mathrm{sign}(\delta)/2$, the convergent advection is represented with a first-order upwind method. For $c = 1/2$, the convergent advection is represented with a second-order centered method. These three choices are summarized in Table 1. Similar tendencies due to δ are applied to momentum and other water species, but the effect of these terms is negligible. Unless specified otherwise, the second-order method ($c = 1/2$) is used for both WTG and WPG.

Simulations are performed using Das Atmosphärische Modell (DAM, Romps 2008), a compressible cloud-resolving model. In all cases, the horizontal grid spacing is 2 km and the domain is doubly periodic. The Coriolis force is omitted, as is appropriate for circulations

on the equator. Steady-state simulations are performed over an ocean with surface fluxes specified by the bulk aerodynamic formula, and with interactive radiation in which the top-of-the-atmosphere insolation is set to the diurnal average at the equator on January 1. To limit the computational expense of the steady-state simulations, the vertical grid is stretched, ranging from a spacing of about 50 m near the surface to 1 km in the stratosphere. Transient simulations are run with neither surface fluxes nor radiation in order to focus on the short-time response. Since these transient simulations are less computationally expensive, their vertical grid spacing is set to a constant 100 meters.

3. *A priori* test

Consider a steady-state column with average profiles $\bar{\theta}_v$ and $\bar{p}$ that sits in an environment with average profiles θ_{v0} and p_0. Both WTG and WPG make predictions about this column that can be tested *a priori* in a simulation that resolves both the column and the environment. WTG predicts a linear relationship between the vertical advection of virtual potential temperature $w\partial_z\theta_{v0}$ and the virtual temperature difference $\bar{\theta}_v - \theta_{v0}$. WPG predicts a linear relationship between the horizontal divergence δ and the density-weighted pressure difference $(\bar{p} - p_0)/\bar{\rho}$. We can test these proposed relationships in a steady-state cloud-resolving simulation over an ocean with an isolated SST perturbation.

This three-dimensional simulation is run on a bowling-alley domain whose dimensions are 2304 km in x, 8 km in y, and 30 km in z. The SST distribution is constant in y and has a 100-km-wide hot spot in x. The SST distribution, which is shown in the upper-left panel

of Figure 2, is prescribed as

$$T(x,y) \;=\; T_0 + \Delta T \exp\left[-\left(\frac{x-x_0}{L/2}\right)^n\right] \tag{7}$$

with $T_0 = 298$ K, $\Delta T = 4$ K, $n = 8$, and $L = 100$ km. To achieve a steady state, the simulation is run for two months; the first month is discarded as spin up and averages are taken over the second month.

Figure 1 shows the buoyancy $B = (\langle\rho\rangle/\rho - 1)g$, pressure perturbation $(p - \langle p\rangle)/\langle\rho\rangle$, horizontal velocity u, and vertical velocity w. Here, all variables are averaged over the 8 km of y and the one month of time, but the angled brackets denote an additional average over x. The two dotted vertical lines denote the 100-km-wide column over the SST hot spot. The panels are arranged in order of causality according to the WPG paradigm: from top to bottom, the buoyancy perturbations generate pressure perturbations by hydrostatic balance, and these pressure perturbations drive inflow and outflow, which, by continuity, determine the vertical velocity.

Among the stand-out features in Figure 1 is the three-layer outflow pattern, with horizontal velocities of several meters per second. This same pattern is also present in daily averages, so this is truly a steady-state circulation. This type of layered outflow is not unique to these simulations: see the two-layer outflow in Figure 4a of Blossey et al. (2010), the three-layer outflow in Figure 4b of Bretherton et al. (2006), and the six-layer outflow in Figure 5a of Bretherton et al. (2006). A hint of a two-layer outflow is also seen in Figure 9 of Raymond (1994), which uses parameterized convection.

Also note-worthy is the layered pattern of steady-state buoyancy. The magnitude of the buoyancy structure is about 1–2 cm s^{-2}, which corresponds to a virtual-temperature

anomaly of about 0.5 K. Peak to trough, this corresponds to a virtual-temperature variation of about 1 K. This is the same scale of virtual-temperature variation found in other bowling-alley simulations; for example, see Figure 10 of Raymond (1994), Figures 6a, 7a, and 8a of Grabowski et al. (2000), and Figure 6 of Bretherton et al. (2006).

In contrast to the structure in the top three panels, the bottom panel shows that the vertical velocity is everywhere positive in the 100-km-wide column atop the hot spot. This falsifies the basic premise of the relaxed form of WTG, which states that negatively buoyant air should sink (see equation 1). A similar point was made by Romps (2012) in the context of analytical solutions to the Boussinesq equations. From the middle two figures, we see that the horizontal Laplacian of p matches up well with the divergence of u, in agreement with the WPG approximation.

These conclusions can be reached more definitively by looking at mean profiles. The middle-left panel of Figure 2 plots two quantities normalized by their maximum absolute value: the density-weighted difference between p inside and outside the 100-km column, and the net horizontal divergence in the column. According to WPG, these two curves should be proportional to one another, and we see that this is largely true. Pairs of peaks are offset somewhat in the vertical, and a near-surface mean wind (visible in the third panel of Figure 1) has displaced the surface convergence outside of the 100-km column. Nevertheless, it is clear, as it is from Figure 1, that the extrema of Δp are roughly colocated with the extrema of δ. Using a steady-state version of equation (3), we can read off the Rayleigh drag α by taking the ratios of local extrema, which are indicated by the dots on the curves. In particular, we calculate $(\bar{p} - p_0)/(L^2 \bar{\rho} \bar{\delta})$, where a bar denotes a horizontal and temporal average in the column, a subscript 0 denotes a horizontal and temporal average in the rest

of the domain, and $L = 100$ km is the width of the column. For the four pairs of extrema, this gives four values for α that range from 1.2×10^{-5} s^{-1} to 5.2×10^{-5} s^{-1}, with a mean of 2.8×10^{-5} s^{-1}. This corresponds to a Rayleigh damping time of 10 hours.

To test the sensitivity of this result to changes in the shape of SST and size of the column, a second simulation is run using equation (7) with $T_0 = 298$ K, $\Delta T = 4$ K, $n = 2$, and $L = 500$ km. This SST distribution is shown in the upper-right panel of Figure 2. Producing vertical plots of pressure difference and divergence for the column inside the vertical dotted lines, we get the results in the middle-right panel of Figure 2. This time, the surface convergence is well within the column, so the pressure difference and divergence agree well there. Further aloft, the extrema continue to be colocated, but their ratios cover a wider range.

The bottom row of Figure 2 plots three quantities for each simulation: normalized profiles of $\bar{w}\partial_z\bar{\theta}$, $\bar{\theta}_v - \theta_{v0}$, and $\bar{\theta} - \theta_0$. As before, bars denote an average over the column and the subscript 0 denotes an average over the rest of the domain. Since $\partial_z\bar{\theta}$, $\partial_z\bar{\theta}_v$, $\partial_z\theta_0$, and $\partial_z\theta_{v0}$ are nearly identical, the results are independent of which is chosen for the WTG relationship; here, $\partial_z\bar{\theta}$ is chosen for plotting. According to relaxed WTG, the vertical advection of potential temperature $\bar{w}\partial_z\bar{\theta}$ is proportional to the virtual temperature difference $\bar{\theta}_v - \theta_{v0}$, but no such proportionality is seen in these figures. In particular, WTG assumes the ratio $(\bar{\theta}_v - \theta_{v0})/(\bar{w}\partial_z\bar{\theta})$ is a constant τ, which is interpreted as a gravity-wave propagation time. Since $\bar{\theta}_v - \theta_{v0}$ oscillates around zero with height, the diagnosed τ also oscillates between positive and negative values, which invalidates the interpretation of τ as a physical timescale. Using $\bar{\theta} - \theta_0$ in the WTG equation would only make matters worse: τ would be mostly negative. Fundamentally, this problem is caused by WTG's assumption that light fluid rises and heavy fluid sinks. From the plots of $\bar{\theta}_v - \theta_{v0}$, we see that the ascending column is ac-

tually a stack of positively and negatively buoyant layers. This agrees with the analysis of Romps (2012): we generally expect columns with steady-state ascent to have little, if any, column-integrated buoyancy. Therefore, since the ascending column is more humid than its surroundings, the ascending column must be mostly *colder* than its surroundings (i.e., $\bar{\theta} - \theta_0 < 0$) to offset the virtual temperature effect of its humidity.

4. *A posteriori* test: steady state

In the first *a posteriori* test, we try to replicate the bowling alley's large-scale dynamics with WTG and WPG. In particular, DAM is run on a doubly periodic domain (96 km by 96 km) with an SST equal to the hot-spot peak in the bowling-alley simulation (302 K). In the bowling-alley simulation, convergence generates a mean wind of 0.9 m s^{-1} at the surface; to account for this in the WTG and WPG simulations, a wind vector of $(0.9, 0.0)$ m s^{-1} is added to the surface wind in the bulk aerodynamic formula for surface enthalpy fluxes. The reference profiles p_0 (for WPG) and θ_{v0} (for WTG) are calculated from the horizontal average of the bowling-alley simulation outside the 100-km column. Convergent advection is modeled using the second-order method ($c = 1/2$), which gives the best results for both WTG and WPG; the sensitivity to this choice is discussed below. Each simulation is run for at least one month and averages are taken over all but the the first week, which is discarded as spin up. The success of the WTG and WPG approximations will be measured by the extent to which these simulations replicate the behavior of the bowling-alley column.

Before we begin, we must also choose values for the parameters τ (for WTG) and α^* (for WPG). Fortunately, theory provides some guidance on the order of magnitude to use

for these parameters. In an analysis of the Boussinesq equations, Romps (2012) finds that the WTG parameter τ should be set to $\alpha(\pi L/NH)^2$ when studying steady-state solutions; here, α is the Rayleigh drag, L is the horizontal scale of the column, N is the Brunt-Väisälä frequency, and H is the vertical scale of the troposphere. With $\alpha = 2.8 \times 10^{-5}$ s^{-1} (the value diagnosed from the bowling-alley simulation), $L = 100$ km, $N = 0.01$ s^{-1}, and $H = 10$ km, this gives $\tau = 5$ minutes. This is the value of τ used in the simulations discussed below. Romps (2012) also shows that WPG should use $\alpha^* = \alpha$ when studying steady-state solutions. This gives $\alpha^* = 2.8 \times 10^{-5}$ s^{-1} (i.e., $1/\alpha^* = 10$ hours), which is used along with $L = 100$ km in equation (3) for these simulations.

Figure 3 shows the mean vertical velocities in the 100-km-wide column of the bowling alley (black) and in WTG (thick dotted red) and WPG (thick dashed blue). The bowling-alley column has a vertical velocity that rises with smooth undulations to a maximum of 10 cm s^{-1} at 9.1 km, and then decreases smoothly to zero around 12 km. WPG exhibits a similar profile that is everywhere non-negative with a smooth increase to a maximum of 11 cm s^{-1} at 9.6 km. By contrast, the WTG vertical velocity is more top-heavy with a peak of 22 cm s^{-1} at 10.1 km.

Figure 4 shows the anomaly (with respect to the bowling-alley mean) of the virtual potential temperature in the bowling-alley column, in WPG with $\alpha^* = 10$ hours, and in WTG with $\tau = 5$ minutes. As in the bowling alley, the WPG simulation has stacked layers of positively and negatively buoyant air. This behavior is expected for a column with an anomalous heat source aloft (Romps 2012); here, the heat source is the latent heating from moist convection. WTG does not exhibit this stacked structure; its air is positively buoyant throughout the depth of the ascending troposphere.

To test the sensitivity of the WTG approximation to its parameter τ, the WTG simulation is rerun with $\tau = 30$ minutes. Thirty minutes is roughly the time it would take first-baroclinic waves to exit the column; this is the timescale commonly assigned to τ in implementations of WTG (e.g., Raymond and Zeng 2005). The mean w in this simulation is shown as the thin, red, dotted curve in Figure 3. Changing τ to this standard value worsens several aspects of the simulation: the peak vertical velocity moves up to a height of 11.1 km, and w attains a local minimum of 2 cm s^{-2} where the bowling alley has its peak of 10 cm s^{-2}.

To test the sensitivity of the WPG approximation to its parameter α^*, the WPG simulation is rerun with $1/\alpha^* = 5$ hours. The mean w in this simulation is shown as the thin, blue, dashed curve in Figure 3. Naively, one might expect from the steady-state version of equation (3) that doubling α^* would lead to a halving of δ and, therefore, to a halving of w. Instead, there is almost perfect compensation: the atmosphere adjusts its mean pressure profile such that the pressure anomaly $\overline{p}(z,t) - p_0(z)$ doubles. The reasons for this compensation are unclear. But, given the uncertainties in the value of the Rayleigh damping (either in the bowling-alley simulation or in the real atmosphere), it is reassuring to see that the steady-state WPG simulation is fairly insensitive to this parameter.

We can also explore the sensitivity of WTG and WPG to the way in which the convergent advection is modeled. We repeat the WTG simulation with $\tau = 5$ and the WPG simulation with $1/\alpha^* = 10$ hours using the three different treatments of convergent advection listed in Table 1. The resulting steady-state vertical velocities are shown in Figure 5, which gives the results for WTG in the first row and WPG in the second row. The left, middle, and right columns give the results for no advection ($c = 0$), first-order advection ($c = 1/2 - \text{sign}(\delta)/2$), and second-order advection ($c = 1/2$), respectively. This figure illustrates the high sensitiv-

ity of a column with parameterized supra-domain-scale dynamics to the representation of convergent advection. For a given c, however, the WTG and WPG simulations exhibit some qualitatively similar behavior.

In the case with no convergent advection (left column of Figure 5), there is subsidence below about 4 km and ascent above. The ascent above 4 km coincides with moist convection between 4 and 12 km. Below 4 km, the subsidence coincides with the evaporation of precipitation: the evaporative cooling drives the subsidence, while the subsidence maintains the subsaturation needed for evaporative cooling. The top of the subsiding layer sits at the melting line, where the removal of sensible heat by the melting of solid hydrometeors provides a substantial and abrupt cooling.

In the case with a first-order treatment of convergent advection (middle column of Figure 5), there is subsidence throughout most of the troposphere. Deep convection is completely inhibited by the "upwind" advection of dry, environmental air into the column. Without the possibility of feedbacks between moist convection and the SDS dynamics, the column must subside at the rate required to balance radiative cooling, so the WTG and WPG profiles of w are nearly identical. Below 1 km, the column's warmer SST leads to a warmer boundary layer compared to the column's environment, and this drives ascent. Cloud base is at 1 km with scattered cumulus between 1 and 2 km.

In the case with a second-order treatment of convergent advection (right column of Figure 5), there is ascent throughout the troposphere, with the exception of some slight descent around 12.5 km in the WTG simulation. The ascent coincides with deep convection that extends from a cloud base around 1 km to a height of about 13 km. These profiles are the

same as the thick dashed and dotted profiles in Figure 3.

5. *A posteriori* test: transients

In the second *a posteriori* test, we try to replicate the bowling alley's transient behavior with WTG and WPG. These simulations are initialized with a motionless atmosphere and a patch of positive buoyancy confined to a 100-km-wide column. Compared to the previous sections, the domains used here have a lower model top and a finer vertical grid spacing. For the bowling-alley simulation, the domain is 2304 km in x, 8 km in y, and 20 km in z, with a 2-km horizontal grid spacing and a 100-m vertical grid spacing. For the small domains with WTG and WPG, the domain dimensions are the same as the bowling-alley column (100 km in x, 8 km in y, and 20 km in z) with the same grid spacings of 2 km and 100 m in the horizontal and vertical directions, respectively. These domains are illustrated in Figure 6. Unlike the steady-state simulations in the previous sections, these simulations use neither surface fluxes nor radiation, allowing us to focus on the transient behavior.

For these transient simulations, the reference atmosphere is shown in the left panel of Figure 7. The initial atmosphere is set to have a lapse rate of 6.5 K km^{-1} below 2 km. Above 2 km, $\partial_z \theta_v$ is held constant to simplify the interpretation of the results from WTG, whose equations include a $\partial_z \theta_v$. The humidity is set to zero everywhere and the vertical distribution of density is chosen to give hydrostasy. This virtual potential temperature is used as the reference profile for the WTG simulation, and the corresponding hydrostatic pressure field is used as the reference profile for the WPG simulation.

Since these are transient simulations, we cannot use the same values of τ and α^* that

are used in the previous section: as shown by Romps (2012), the optimal parameters for transient and steady-state solutions are not the same. In the context of the Boussinesq equations, Romps (2012) shows that WTG should use $\tau = \pi L/NH$ to most accurately capture transient behavior; here, L is the horizontal scale of the column, N is the Brunt-Väisälä frequency, and H is the vertical scale of the troposphere. Using $H = 10$ km, $N = 0.01$ s^{-1}, and $L = 100$ km, this expression gives $\tau = 50$ minutes. Since this is derived from the Boussinesq theory and the values used here are approximate, several WTG simulations were run to find the optimal value of τ. The best results were obtained with $\tau = 30$ minutes, which is the value of τ used in the results below. For WPG, the analysis of Romps (2012) shows that the WPG parameter α^* should be set to $2HN/\pi L$ to most accurately capture transient behavior. This gives $\alpha^* = 6 \times 10^{-4}$ s^{-1} if we use the same values as above. Again, this is only an order-of-magnitude estimate, so several WPG simulations were run with this value of α^* and different values of the L in equation (3). The best results were obtained with $L = 35$ km, which is the value of L used in the results below. Similar results were also found using other pairs of α^* and L, including $\alpha^* = 2 \times 10^{-4}$ s^{-1} and $L = 70$ km.

To initiate a transient large-scale circulation in the bowling-alley simulation, the temperature is incremented by 1 K in a patch that covers 100 km in x, the full 8 km in y, and from 2.4 km to 7.4 km in z. In the WTG and WPG simulations, the temperature is incremented by 1 K for all x and y (i.e., 100 km by 8 km) and between 2.4 km and 7.4 km in z. These patches are indicated by the grey boxes in Figure 6. The humidity and temperature profiles in these perturbed columns are shown in the middle panel of Figure 7. To break the symmetry, noise is added to the temperature field everywhere below 1500 meters; in the bowling-alley simulation, this is done both inside and outside the perturbed

column. In particular, the temperature in each grid cell is incremented by a random amount drawn from a uniform probability distribution over -0.03 K to 0.03 K.

These transient simulations are run for one day with no surface fluxes and no radiative cooling. Therefore, there are no diabatic heating sources (no surface fluxes, no radiation, and no release of latent heat because the atmosphere is dry). This makes the final equilibrated state trivial to predict. Since the area ratio of perturbed column to whole domain is very small in the bowling-alley run, we can neglect the small temperature change caused by compensating subsidence. By gravity-wave adjustment, the warm patch will erase its temperature perturbation by adiabatic expansion, leading the warm patch to rise by a distance equal to

$$\frac{\Delta T}{g/c_p - \Gamma},$$

where $\Delta T = 1$ K and $\Gamma = 6.5$ K/km. This predicts a net ascent of about 300 meters.

After one day of simulation, all three simulations have reached a relatively motionless hydrostatic equilibrium. (Note that, for the bowling-alley simulation, this is consistent with a Rayleigh damping time of about 10 hours.) To keep track of the net ascent, the mean vertical velocity at each height in the perturbed column is integrated in time. The profile of net vertical displacement after one day is shown by the dashed curves in the second column of Figure 8 (the dashed curve for WTG is perfectly obscured by the solid curve, which will be discussed momentarily). The horizontal dotted lines at 2.4 km and 7.4 km denote the boundaries of the initial warm patch. As expected, all three dry simulations show a net ascent of the warm patch by about 300 meters after one day.

Although all three simulations agree on the final state, they do not all agree on how they

got there. The dashed curves in the first column of Figure 8 shows the net displacement accrued during the first and second hours (i.e. the "Hour 1" curves are $\int_0^{3600} dt\, w$ and the "Hour 2" curves are $\int_{3600}^{7200} dt\, w$). Both the bowling-alley simulation and the WPG simulation show a broad and smooth region of ascent from the surface up to about 10 km in the first hour, while the WTG simulation shows ascent restricted to the original top-hat warm patch. In the second hour, the bowling-alley and WPG simulations show lobes of descent in the couple kilometers above and below the original warm patch, while the WTG simulation shows only ascent. These descending lobes are expected physically: in the first hour, the warm patch has lifted the air above and below it in a broad first-baroclinic circulation; in the second hour, shallower baroclinic circulations develop to allow those negatively buoyant lobes to descend.

As we see from these dry simulations, both the bowling-alley and WPG simulations exhibit nonlocal responses to a localized heating, while WTG does not. As discussed by Romps (2012), the inability of WTG to produce a nonlocal response could cause it to miss important feedbacks on the convective heating. For example, if the ascent generated below a warm patch could adiabatically cool a convective inhibition layer overlying humid air, then this might trigger additional moist convection, which, through its diabatic heating, could fundamentally alter the transient response.

To test this, another set of simulations are run with dry air above 2 km as before, but saturated air below 2 km. This puts the moist layer 400 meters below the warm patch. The same profiles of θ_v are used, but the density is recalculated to guarantee hydrostatic balance. The humidity and temperature profiles of the perturbed columns in these moist simulations are shown in the right panel of Figure 7.

The results of these moist simulations are shown by the solid curves in Figure 8. Since the WTG method produces only a local response to buoyancy perturbations, the vertical displacement during hour 1, hour 2, and the entire day (bottom row of the figure) are exactly the same as in the dry simulation. In hour 1 of the bowling-alley and WPG simulations, the vertical displacement is also nearly identical to that in the dry case. In hour 2, however, there are distinct differences between the dry and moist cases below 4 km; this is due to the latent-heat release from moist convection that is triggered by the forced ascent below 2 km. At the end of one day, the net vertical displacement of the bowling-alley and WPG simulations both show a maximum in vertical displacement at a height of about 1 km, which is well below the initial temperature perturbation. Since WTG does not generate any nonlocal ascent, it is unable to produce this triggered convection.

6. Conclusions

The weak temperature gradient (WTG) and weak pressure gradient (WPG) schemes are designed to parameterize the large-scale dynamical interaction between a perturbed column and its larger environment. As such, they make testable predictions. For example, the relaxed form of WTG predicts that profiles of steady-state buoyancy and vertical velocity are related by a positive timescale related to gravity-wave propagation. A cloud-resolving simulation with an SST hot spot invalidates this prediction: the diagnosed WTG timescale τ oscillates in height between positive and negative values. WPG, on the other hand, predicts that the steady-state convergence and pressure perturbations are related by a positive Rayleigh-drag coefficient α. This prediction fares relatively well: a tight correlation is found

between these two quantities, with a diagnosed Rayleigh damping timescale $1/\alpha$ of about 10 hours.

In both of the *a posteriori* tests, three types of cloud-resolving simulations are performed: one on a large bowling-alley domain in which a perturbed column and its environment are resolved, one on a domain containing only the perturbed column and using WTG to parameterize the interactions with the larger environment, and a similar simulation with WPG. In the first of these tests, all three simulations are run to a steady state corresponding to an atmospheric column over an SST hot spot. WPG produces a w profile that matches the shape and magnitude of the w profile over the hot spot in the bowling-alley simulation. WTG, on the other hand, produces a w profile that is too top-heavy.

In the second *a posteriori* test, the column is initialized with a positive buoyancy perturbation. The transient w profile of the WPG simulation agrees exceptionally well with the transient w profile in the column of the bowling-alley simulation. One of the key features seen in both simulations is the transient ascent above and below the buoyancy perturbation. WTG does not capture this transient behavior; its w transients are strictly confined to the location of the original buoyancy anomaly. When moisture is added to the simulations, the bowling-alley and WPG simulations both predict the triggering of moist convection, which further heats the column and leads to additional ascent. Since WTG is unable to generate adiabatic lifting below a buoyancy perturbation, it generates no such convective heating and, therefore, errs qualitatively on its prediction of the column's net ascent.

These numerical simulations confirm several of the conclusions that Romps (2012) reached by analysis of linearized Boussinesq equations. In particular, Romps (2012) concluded that a heated column can have steady-state ascent even though the column has no column-

integrated buoyancy; a generic feature of such a state is a vertically oscillating pattern of positive and negative buoyancy. As shown in Figures 1 and 2, cloud-resolving bowling-alley simulations exhibit this behavior: even though the buoyancy oscillates between positive and negative values with height, the vertical velocity is everywhere non-negative. Another conclusion of Romps (2012) is that a buoyancy perturbation aloft can generate adiabatic lifting below, which could potentially trigger moist convection. As shown in Figure 8, a cloud-resolving bowling-alley simulation can exhibit this behavior. The fact that WPG reproduces these phenomena affirms its use as a parameterization of supra-domain-scale (SDS) dynamics.

Acknowledgments

This work was supported by the Laboratory Directed Research and Development Program of Lawrence Berkeley National Laboratory under U.S. Department of Energy Contract No. DE-AC02-05CH11231. The numerical simulations were performed on the Lawrencium cluster provided by the IT Division at the Lawrence Berkeley National Laboratory and the Hopper cluster provided by the National Energy Research Scientific Computing Center, both of which are supported by the Office of Science of the U.S. Department of Energy under Contract No. DE-AC02-05CH11231. Thanks are due to Nadir Jeevanjee, David Raymond, Kyongmin Yeo, and two anonymous reviewers for their feedback on the manuscript.

REFERENCES

Blossey, P. N., C. S. Bretherton, and M. C. Wyant, 2009: Subtropical low cloud response to a warmer climate in a superparameterized climate model. Part II: Column modeling with a cloud resolving model. *Journal of Advances in Modeling Earth Systems*, **1**.

Blossey, P. N., Z. Kuang, and D. M. Romps, 2010: Isotopic composition of water in the tropical tropopause layer in cloud-resolving simulations of an idealized tropical circulation. *Journal of Geophysical Research*, **115**, D24 309, doi:doi:2010/10.1029/2010JD014554.

Bretherton, C. S., P. N. Blossey, and M. E. Peters, 2006: Interpretation of simple and cloud-resolving simulations of moist convection–radiation interaction with a mock-Walker circulation. *Theoretical and Computational Fluid Dynamics*, **20 (5)**, 421–442.

Caldwell, P. and C. S. Bretherton, 2009: Response of a subtropical stratocumulus-capped mixed layer to climate and aerosol changes. *Journal of Climate*, **22 (1)**, 20–38.

Grabowski, W. W., J.-I. Yano, and M. W. Moncrieff, 2000: Cloud resolving modeling of tropical circulations driven by large-scale sst gradients. *J. Atmos. Sci.*, **57 (13)**, 2022–2040, doi:10.1175/1520-0469(2000)057⟨2022:CRMOTC⟩2.0.CO;2, URL `http://dx.doi.org/10.1175/1520-0469(2000)057<2022:CRMOTC>2.0.CO;2`.

Kuang, Z., 2008: Modeling the interaction between cumulus convection and linear gravity waves using a limited-domain cloud system–resolving model. *Journal of the Atmospheric Sciences*, **65 (2)**, 576–591.

Kuang, Z., 2011: The wavelength dependence of the gross moist stability and the scale selection in the instability of column-integrated moist static energy. *Journal of the Atmospheric Sciences*, **68 (1)**, 61–74.

Nilsson, J. and K. A. Emanuel, 1999: Equilbrium atmospheres of a two-column radiative-convective model. *Quarterly Journal of the Royal Meteorological Society*, **125 (558)**, 2239–2264.

Raymond, D. J., 1994: Convective processes and tropical atmospheric circulations. *Quarterly Journal of the Royal Meteorological Society*, **120 (520)**, 1431–1455, doi:10.1002/qj.49712052002, URL `http://dx.doi.org/10.1002/qj.49712052002`.

Raymond, D. J., 2007: Testing a cumulus parametrization with a cumulus ensemble model in weak-temperature-gradient mode. *Quarterly Journal of the Royal Meteorological Society*, **133 (626)**, 1073–1085.

Raymond, D. J. and X. Zeng, 2000: Instability and large-scale circulations in a two-column model of the tropical troposphere. *Quarterly Journal of the Royal Meteorological Society*, **126 (570)**, 3117–3135.

Raymond, D. J. and X. Zeng, 2005: Modelling tropical atmospheric convection in the context of the weak temperature gradient approximation. *Quarterly Journel of the Royal Meteorological Society*, **131 (608)**, 1301–1320.

Romps, D. M., 2008: The dry-entropy budget of a moist atmosphere. *Journal of the Atmospheric Sciences*, **65 (12)**, 3779–3799.

Romps, D. M., 2012: Weak pressure gradient approximation and its analytical solutions. *Journal of the Atmospheric Sciences*, **in review**.

Sessions, S. L., S. Sugaya, D. J. Raymond, and A. H. Sobel, 2010: Multiple equilibria in a cloud-resolving model using the weak temperature gradient approximation. *Journal of Geophysical Research*, **115**, D12 110.

Shaevitz, D. A. and A. H. Sobel, 2004: Implementing the weak temperature gradient approximation with full vertical structure. *Monthly Weather Review*, **132 (2)**, 662–669.

Sobel, A. H. and C. S. Bretherton, 2000: Modeling tropical precipitation in a single column. *Journal of Climate*, **13 (24)**, 4378–4392.

Wang, S. and A. H. Sobel, 2011: Response of convection to relative sea surface temperature: Cloud-resolving simulations in two and three dimensions. *Journal of Geophysical Research*, **116**, D11 119, doi:doi:10.1029/2010JD015347.

Wang, S. and A. H. Sobel, 2012: Impact of imposed drying on deep convection in a cloud-resolving model. *Journal of Geophysical Research – Atmospheres*, **in review**.

List of Tables

1 For equations (5) and (6), the value of c for the three different treatments of "convergent advection". 24

Treatment of convergent advection	
None	$c = 0$
1^{st}-order	$c = \big[1 - \text{sign}(\delta)\big]/2$
2^{nd}-order	$c = 1/2$

TABLE 1. For equations (5) and (6), the value of c for the three different treatments of "convergent advection".

List of Figures

1 For the bowling-alley simulation with a 100-km hot spot, the average (over 8 km of y and 1 month) of buoyancy $B = (\langle\rho\rangle/\rho - 1)g$, pressure perturbation $(p - \langle p\rangle)/\langle\rho\rangle$, horizontal velocity u, and vertical velocity w, where angled brackets denote an additional average over x. Axes are x and z, and vertical dotted lines denote the boundaries of a 100-km-wide column. 27

2 (Top row) The SST distributions used in the two bowling-alley simulations. (Middle row) Normalized profiles of horizontal divergence δ (solid) and pressure perturbation (dashed) averaged over the columns denoted by the dotted lines in the top row. The solid circles denote the extrema used to calculate α. (Bottom row) Normalized profiles of vertical potential-temperature advection, virtual-potential-temperature perturbation, and potential-temperature perturbation for the columns denoted by the dashed lines in the top row. "Normalized" here means divided by the maximum absolute value. 28

3 Steady-state vertical velocity in the bowling alley (solid black), WPG with $1/\alpha^* = 10$ hours (thick dashed blue), WPG with $1/\alpha^* = 5$ hours (thin dashed blue), WTG with $\tau = 5$ minutes (thick dotted red), and WTG with $\tau = 30$ minutes (thin dotted red). 29

4 Steady-state anomaly in virtual potential temperature for the bowling-alley column (black), WPG with $1/\alpha^* = 10$ hours (dashed blue), and WTG with $\tau = 5$ minutes (dotted red). The anomaly is calculated with respect to the average over the entire bowling alley. 30

5 Steady-state vertical-velocity profiles using WTG (top row) and WPG (bottom row) for three different treatments of horizontal advection due to convergence: none, first-order, and second-order. 31

6 The x and z dimensions of the transient bowling-alley, WTG, and WPG simulations. The grey boxes denote the regions initialized to be warmer than their surroundings by 1 K. 32

7 (Left) The virtual potential temperature (solid) and relative humidity (dashed) used as the environment for the dry bowling-alley, WTG, and WPG simulations. (Middle) For the dry runs, the initial state used for the perturbed column of the bowling alley and for the initial state of the WTG and WPG simulations. (Right) For the moist runs, the humidity profile used as the initial condition in the column and the environment, and the virtual potential temperature profile used as the initial condition in the column. 33

8 Net vertical displacements (integrals over time of vertical velocity) for the bowling alley (top row), WPG (middle row), and WTG (bottom row). The left column shows the net displacements generated during the first and second hours to give a sense of the temporal evolution of the column. The right column gives the net displacement during the entire day. Dashed curves are from the dry simulations and solid curves are from the simulations with lower-tropospheric humidity. 34

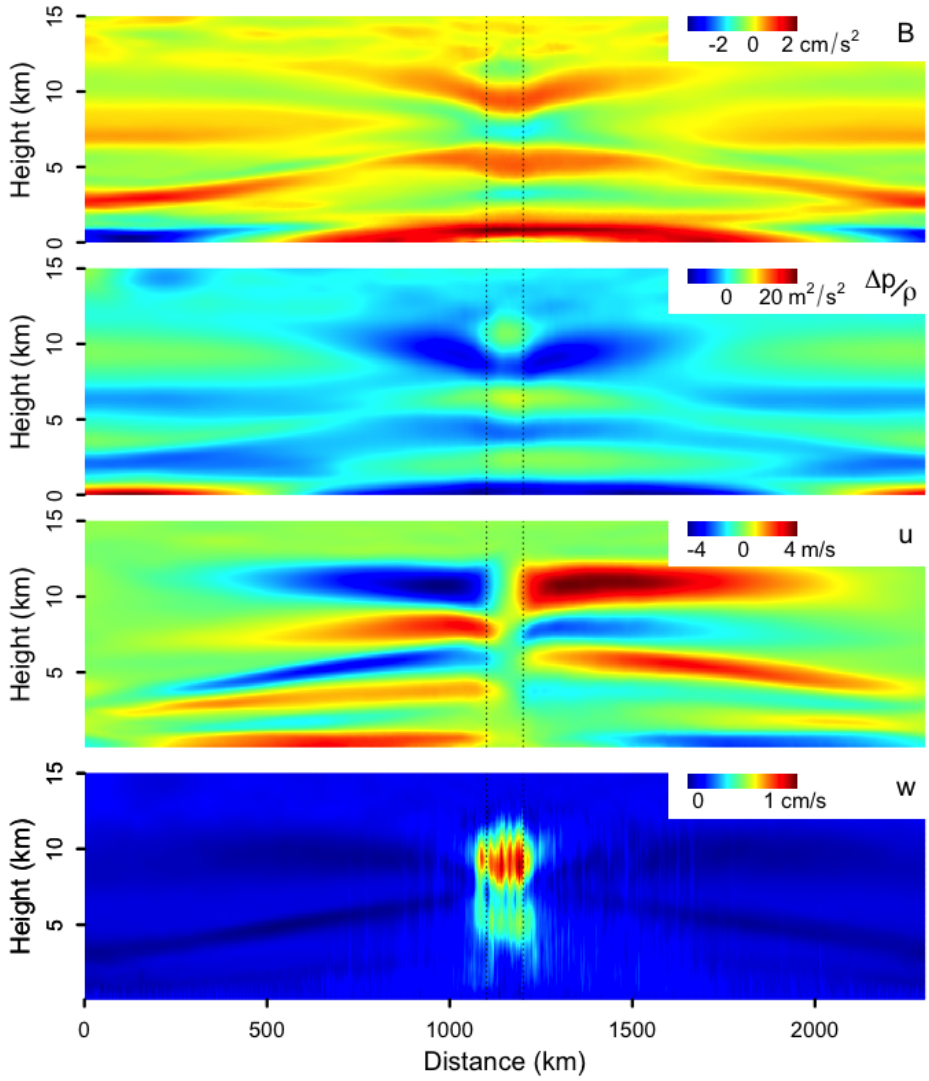

FIG. 1. For the bowling-alley simulation with a 100-km hot spot, the average (over 8 km of y and 1 month) of buoyancy $B = (\langle\rho\rangle/\rho - 1)g$, pressure perturbation $(p - \langle p\rangle)/\langle\rho\rangle$, horizontal velocity u, and vertical velocity w, where angled brackets denote an additional average over x. Axes are x and z, and vertical dotted lines denote the boundaries of a 100-km-wide column.

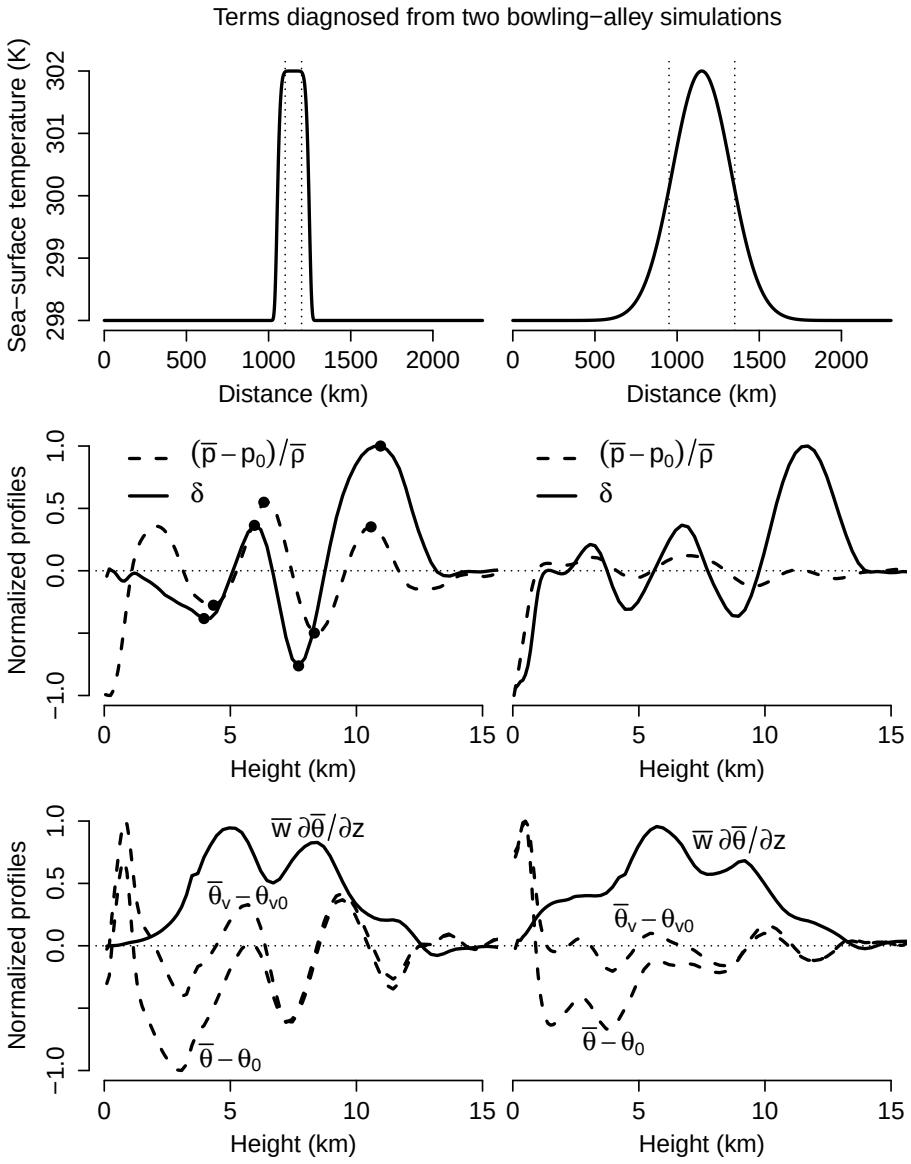

FIG. 2. (Top row) The SST distributions used in the two bowling-alley simulations. (Middle row) Normalized profiles of horizontal divergence δ (solid) and pressure perturbation (dashed) averaged over the columns denoted by the dotted lines in the top row. The solid circles denote the extrema used to calculate α. (Bottom row) Normalized profiles of vertical potential-temperature advection, virtual-potential-temperature perturbation, and potential-temperature perturbation for the columns denoted by the dashed lines in the top row. "Normalized" here means divided by the maximum absolute value.

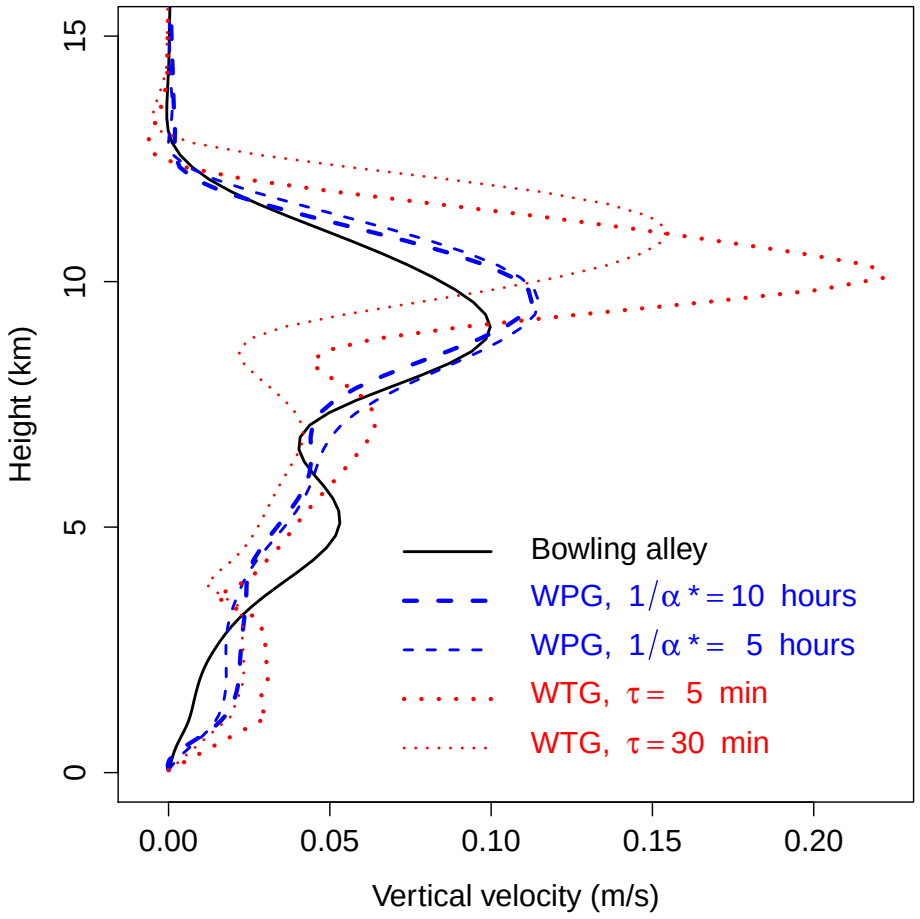

FIG. 3. Steady-state vertical velocity in the bowling alley (solid black), WPG with $1/\alpha^* = 10$ hours (thick dashed blue), WPG with $1/\alpha^* = 5$ hours (thin dashed blue), WTG with $\tau = 5$ minutes (thick dotted red), and WTG with $\tau = 30$ minutes (thin dotted red).

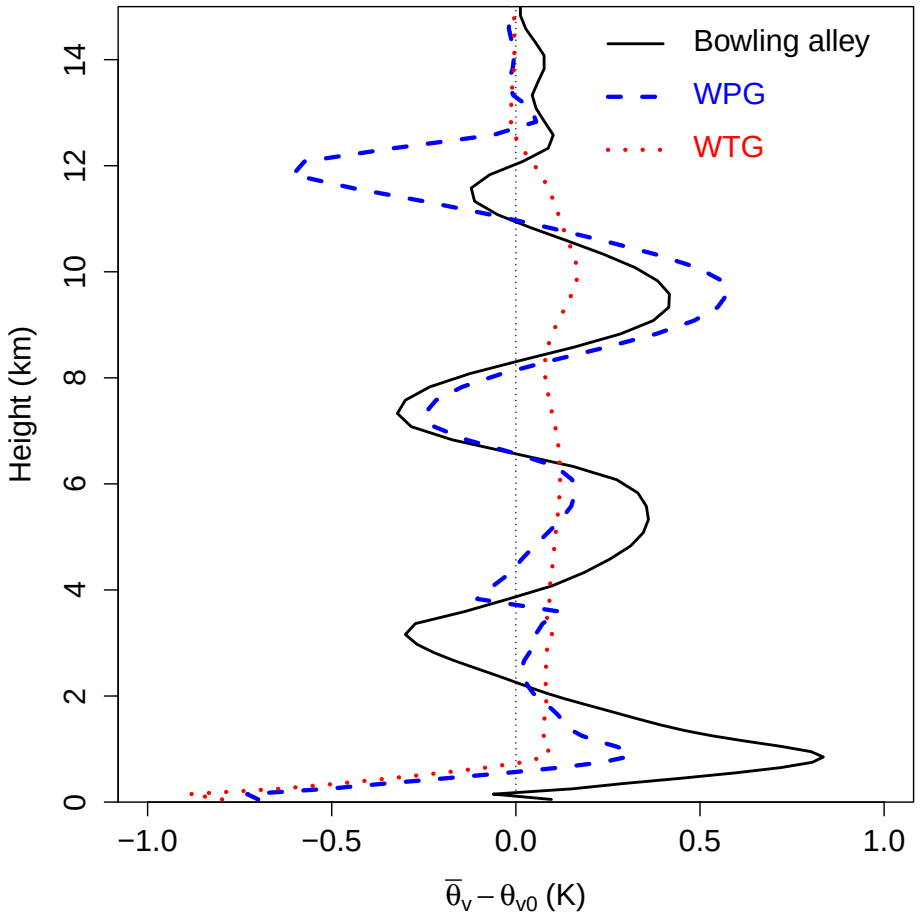

FIG. 4. Steady-state anomaly in virtual potential temperature for the bowling-alley column (black), WPG with $1/\alpha^* = 10$ hours (dashed blue), and WTG with $\tau = 5$ minutes (dotted red). The anomaly is calculated with respect to the average over the entire bowling alley.

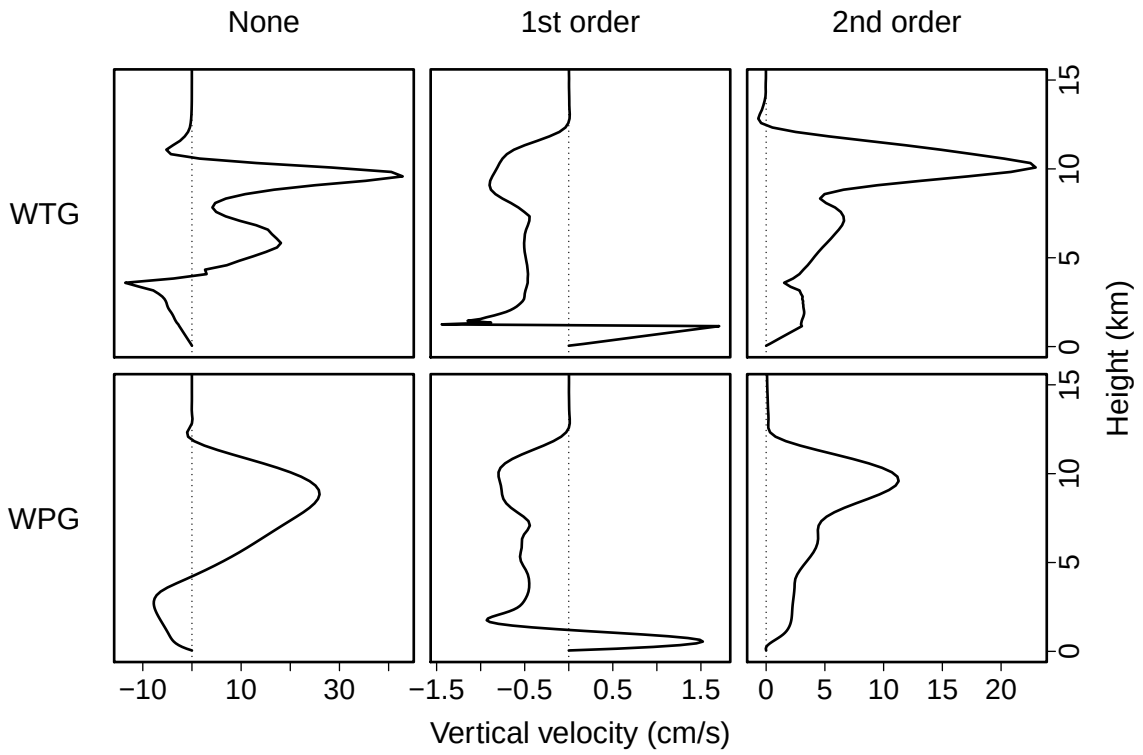

FIG. 5. Steady-state vertical-velocity profiles using WTG (top row) and WPG (bottom row) for three different treatments of horizontal advection due to convergence: none, first-order, and second-order.

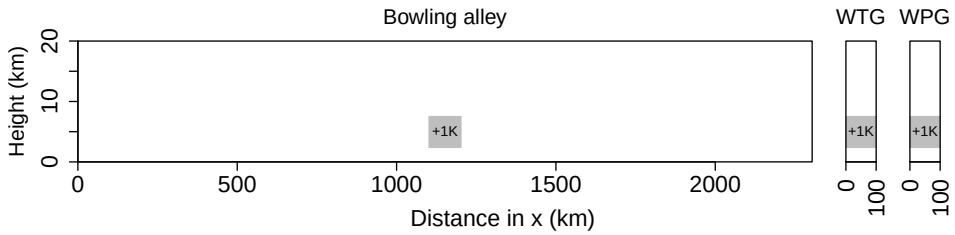

FIG. 6. The x and z dimensions of the transient bowling-alley, WTG, and WPG simulations. The grey boxes denote the regions initialized to be warmer than their surroundings by 1 K.

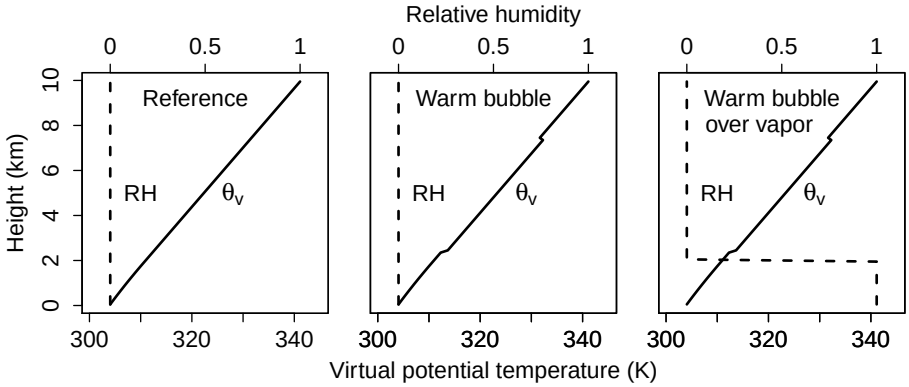

FIG. 7. (Left) The virtual potential temperature (solid) and relative humidity (dashed) used as the environment for the dry bowling-alley, WTG, and WPG simulations. (Middle) For the dry runs, the initial state used for the perturbed column of the bowling alley and for the initial state of the WTG and WPG simulations. (Right) For the moist runs, the humidity profile used as the initial condition in the column and the environment, and the virtual potential temperature profile used as the initial condition in the column.

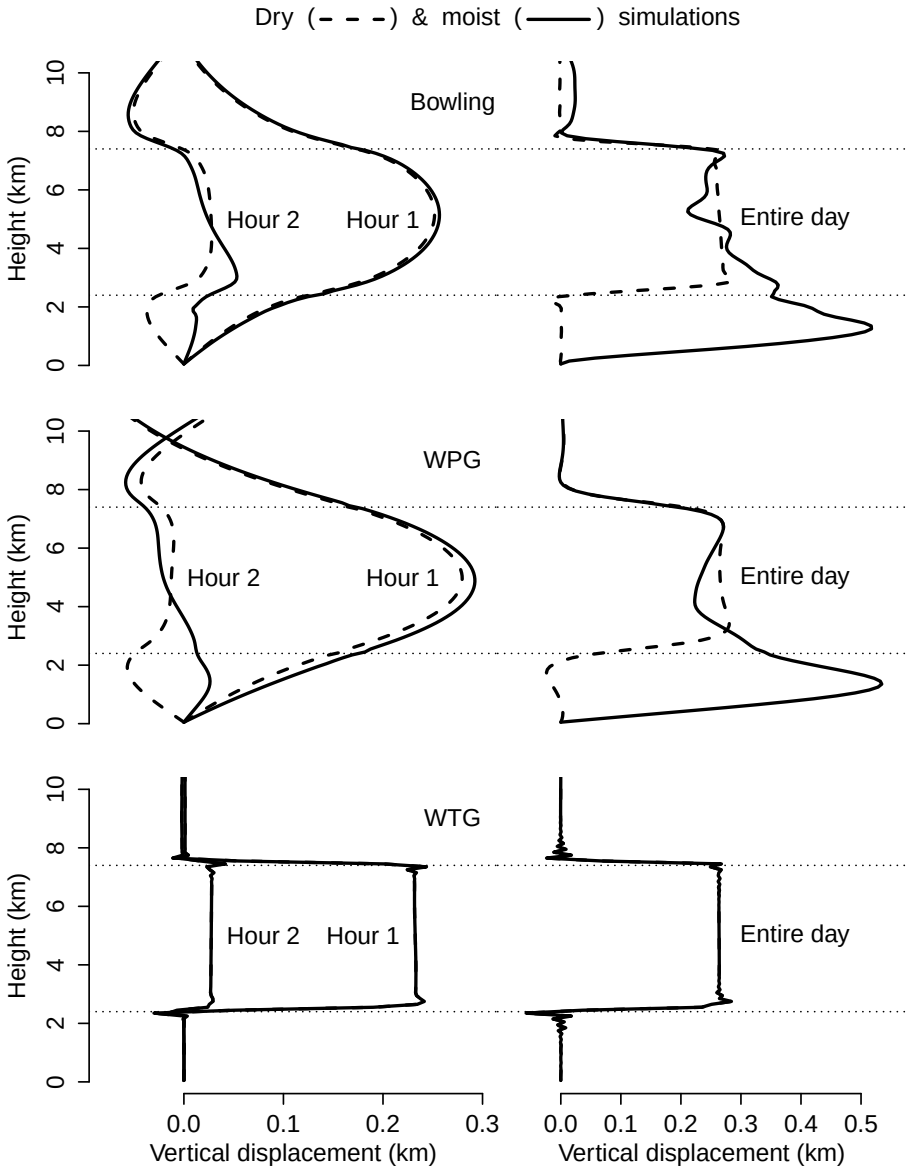

FIG. 8. Net vertical displacements (integrals over time of vertical velocity) for the bowling alley (top row), WPG (middle row), and WTG (bottom row). The left column shows the net displacements generated during the first and second hours to give a sense of the temporal evolution of the column. The right column gives the net displacement during the entire day. Dashed curves are from the dry simulations and solid curves are from the simulations with lower-tropospheric humidity.